Journal of Materials Chemistry A

Conjugated Molecules Based 2D Perovskites for High-Performance Perovskite Solar Cells

Journal:	*Journal of Materials Chemistry A*
Manuscript ID	TA-ART-07-2021-005934.R1
Article Type:	Paper
Date Submitted by the Author:	08-Aug-2021
Complete List of Authors:	Zhu, Tao; University of Akron Shen, Lening; University of Akron Chen, Hanlin; University of Akron Yang, Yongrui; University of Akron Zheng, Luyao; University of Akron Chen, Rui; University of Akron, Polymer Engineering Zheng, Jie; University of Akron, Chemical and Biomolecular Engineering Wang, Junpeng; University of Akron, Polymer Science Gong, Xiong; The University of Akron, Polymer Eng

Conjugated Molecules Based 2D Perovskites for High-Performance Perovskite Solar Cells

Tao Zhu,[1] Lening Shen,[1] Hanlin Chen,[1] Yongrui Yang,[1] Luyao Zheng,[1] Rui Chen,[1] Jie Zheng,[2] Junpeng Wang*,[1] and Xiong Gong*,[1]

1) School of Polymer Science and Polymer Engineering, 2) Department of Chemical, Biomolecular and Corrosion Engineering, College of Engineering and Polymer Science, The University of Akron, Akron, OH 44325, USA

ABSTRACT

Conjugated molecules have been typically utilized as either hole or electron extraction layers to boost the device performance of perovskite solar cells (PSCs) by three-dimensional (3D) perovskites due to their high charge carrier mobility and electrical conductivity. Conjugated molecules, however, functionalize as the passivation role in creating two-dimensional (2D) perovskites was rarely reported. In this study, we report novel conjugated aniline 3-phenyl-2-propen-1-amine (PPA) based 2D perovskites and further demonstrate efficient and stable PSCs by the $(PPA)_x(MAPbI_3)_{1-x}/MAPbI_3$ bilayer thin film (where MA is $CH_3NH_3^+$). The $(PPA)_x(MAPbI_3)_{1-x}/MAPbI_3$ bilayer thin film possesses superior crystallinity and passivated trap states, resulting in enhanced charge transport and suppressed charge carrier recombination compare to 3D $MAPbI_3$ thin film. As a result, PSCs by the $(PPA)_x(MAPbI_3)_{1-x}/MAPbI_3$ bilayer thin film exhibit a power conversion efficiency (PCE) of 21.98%, which is approximately 25 % enhancement compared to that by $MAPbI_3$ thin film. Moreover, un-encapsulated PSCs by the $(PPA)_x(MAPbI_3)_{1-x}/MAPbI_3$ bilayer thin film retains 50% of their initial PCEs after 1200 hours in the ambient atmosphere (25 °C, and 30 ± 10 humidity), whereas PSCs by 3D $MAPbI_3$ thin film shows a significant degradation after 100 hours and degrades more than 50% of their original PCEs after 500 hours. These results demonstrate that the incorporation of conjugated molecules as organic spacer cations to create 2D perovskite on top of 3D perovskite is an effective way to approach high-performance PSCs.

KEYWORDS: 2D perovskites, conjugated organic molecule, organic spacer, perovskite solar cells, efficiency, and stability

*Corresponding authors, e-mails: xgong@uakron.edu (XG); jwang6@uakron.edu (JPW); Fax: (330) 9723406

1. INTRODUCTION

Three-dimensional (3D) organic-inorganic metal halide hybrid perovskites are promising photovoltaic materials due to their unique optoelectronic properties.[1-11] A state-of-the-art perovskite solar cell (PSC) has been certified to exhibit an astonishing power conversion efficiency (PCE) of 25.5%.[12] However, 3D perovskites are quite sensitive to moisture and oxygen, resulting in a significant degradation in the ambient atmosphere. Thus the long-term stability of PSCs by 3D perovskites is a major bottleneck issue for their practical applications.[13,14] In comparison with 3D perovskites, two-dimensional (2D) perovskites have been developed to approach stable PSCs.[15] Studies indicated that the utilization of a small amount of large-sized organic cations to replace regular smaller cations in the perovskite precursors to form a 2D perovskite passivation layer on the top of 3D perovskite was a facile way to boost both the efficiency and stability of PSCs.[16-21] With phenethylammonium iodide (PEAI) to treat the surface of 3D perovskite, You et al. found out that PEAI-based 2D perovskites could reduce surface defects and suppress surface non-radiative recombination, resulting in enhanced PCEs.[19] Chen et al.[21] demonstrated that the 2-thiophenemethylammonium cations can be successfully embedded into 3D perovskites, resulting in enlarged crystallinity and orientated 2D/3D perovskite bilayer thin films. Recently, we reported novel propargylamine-based quasi-2D perovskite thin films and further demonstrated efficient and stable PSCs with dramatically suppressed photocurrent hysteresis.[15] While impressive device performance has been reported for PSCs by the 2D/3D perovskite bilayer thin films, 2D perovskites based on the insulating organic molecules possess poor charge transport, restricting the device performance of PSCs.[22-28]

Conjugated organic molecules have received considerable attention as the hole and/or electron transport layers in PSCs by 3D perovskite thin films due to their high charge carrier mobility and electrical conductivity compared to those insulating organic molecules.[29,30] But conjugated organic molecules used to create 2D perovskites were rarely reported. Hence, it is reasonable to develop conjugated organic molecule-based 2D perovskites for boosting the device performance of PSCs by the 2D/3D perovskite bilayer thin film. The advantages of high charge carrier mobility of conjugated molecules and high stability of 2D perovskites are highly imperative to ultimately balance the efficiency and stability of PSCs by the 2D/3D perovskite bilayer thin film.

In this work, we report efficient and stable PSCs by the 2D/3D perovskite bilayer thin film, where 2D perovskite thin layer is created by using an innovative conjugated aniline 3-phenyl-2-propen-1-amine (PPA) as the organic space cations. The $(PPA)_x(MAPbI_3)_{1-x}/MAPbI_3$ perovskite bilayer thin film (where MA is $CH_3NH_3^+$) possesses larger crystallinity and passivated trap states, leading to enhanced charge transport and suppressed charge carrier recombination compared to 3D $MAPbI_3$ thin film. As a result, PSCs by the $(PPA)_x(MAPbI_3)_{1-x}/MAPbI_3$ bilayer thin film exhibit a PCE of 21.98% and significantly boosted stability in the ambient atmosphere. Our results demonstrate that the incorporation of conjugated molecules as organic spacer cations to create 2D perovskite on top of 3D perovskite is an effective way to approach high-performance PSCs.

2. EXPERIMENTAL SECTION

2.1 Materials

Gamma-butyrolactone (GBL, 99%), methylamine (MA) (33 wt % in absolute ethanol), anhydrous acetonitrile (ACN, 99.8%), poly[bis(4-phenyl)(2,4,6-trimethylphenyl)amine] (PTAA), dimethylformamide (DMF, anhydrous, 99.8%), dimethyl sulfoxide (DMSO, anhydrous, 99.9%), toluene (anhydrous, 99.8%), bathocuproine (BCP, 99.99%), aluminum (Al) and silver (Ag) slugs were purchased from Sigma Aldrich. Lead iodide (PbI_2, 99.9985% metals basis) was purchased from Alfa Aesar. C_{60} (99.95% carbon powder) was purchased from Purec60oliveoil. Methyl-ammonium iodide (MAI) was purchased from Greatcell Solar. All materials are used as received without any further treatment. 3-phenyl-2-propen-1-amine (PPA) is synthesized in our laboratory. The details of the synthesis procedures and characterization of PPA are described in the **Supporting Information** (**SI 1**).

2.2 Preparation of Precursor Solution

$MAPbI_3$ perovskite solution: PbI_2 and MAI (molar ratio 1:1) were dissolved in GBL and stirred at 80 °C for over 2 hours (hrs) to form a 1.2 M solution. The solution was filtered into a vial and placed into an oil bath at 110 °C for several hrs until black crystals precipitated at the bottom of the vial. The black $MAPbI_3$ crystals were washed with isopropanol and dried three times. Then, a certain amount of $MAPbI_3$ crystals was placed in a vial, which was then sealed into a bottle containing methylamine solution and kept for over 2 hrs. Methylamine gas in the bottle diffused into the vial and reacted with $MAPbI_3$ crystals, resulting in liquid perovskite intermediate ($MAPbI_3$). Subsequently, $MAPbI_3$ crystals were dissolved into ACN to form a $MAPbI_3$ ACN solution.

The PPA solution: PPA solution was prepared by dissolving the as-synthesized PPA into ACN with different concentrations.

The $(PPA)_x(MAPbI_3)_{1-x}/MAPbI_3$ perovskite solution: a certain amount of (to adjust the ratios of PPA to $MAPbI_3$) PPA solution was mixed with $MAPbI_3$ ACN solution.

2.3 Preparation and Characterization of Perovskite Thin Film

The pre-cleaned quartz (or glass) substrates were treated by UV-ozone plasma for about 20 minutes (mins). The $MAPbI_3$ thin film or $(PPA)_x(MAPbI_3)_{1-x}/MAPbI_3$ bilayer thin film was prepared by spin-cast method with a spin speed of 4000 RPM for 30 seconds (s) from the corresponding solution described above. After that, all thin films were thermally annealed at 100 ^oC for 10 mins and then cooled down to room temperature (RT) naturally.

The X-ray diffraction (XRD) patterns were obtained by a Rigaku Smartlab. The UV-visible absorption spectra were characterized by a Lambda 900 UV-Vis-NIR spectrophotometer (PerkinElmer, Waltham, MA, USA). The photoluminescence (PL) spectra were obtained from QuantaMaster 2361 (HORIBA). The scanning electron microscopy (SEM) images were obtained from field emission scanning electron microscopy (Model JEOL-7401). The film thicknesses were measured by using a Bruker DektakXT Stylus Profilometer with a scan rate of 0.03 mm s^{-1}.

2.4 Fabrication and characterization of PSCs

The pre-cleaned ITO/glass substrates were treated by UV-ozone plasma for about 20 mins, where ITO is indium tin oxide. Then, a ~ 20 nm PTAA thin film was spin-casted on the top of ITO/glass substrates with a spin speed of 6000 RPM for 30 s from 2 mg/mL PTAA toluene solution, followed by thermal annealing at 100 ^oC for 10 mins. After PTAA coated substrates were cooled down to RT, either $MAPbI_3$ or $(PPA)_x(MAPbI_3)_{1-x}/MAPbI_3$ thin films were prepared by the methods described above. Afterward, ~ 40 nm C_{60} and ~8 nm BCP were

sequentially thermally deposited on the top of either $MAPbI_3$ thin film or the $(PPA)_x(MAPbI_3)_{1-x}/MAPbI_3$ bilayer thin film in a vacuum system with a base pressure of 4 x 10^{-6} Torr. PSCs were completed by thermal deposition of ~100 nm Al on the top of the BCP layer in a vacuum system. The device area was measured to be 0.043 cm^2.

The current densities versus voltages (J-V) characteristics of PSCs were tested by a Keithley model 2400 source unit. The light source was a Newport Air Mass 1.5 Global (AM1.5G) full spectrum simulator with a light intensity of 100 $mW \cdot cm^{-2}$, which was calibrated by utilizing a mono-silicon detector (with a KG-5 visible color filter) from the National Renewable Energy Laboratory to reduce the spectral mismatch. The external quantum efficiency (EQE) spectrum was obtained on the solar cell quantum efficiency measurement system (QEX10). The impedance spectroscopy (IS) was conducted using an HP 4194A impedance/gain-phase analyzer under illumination and in dark, at the voltage closing to an open-circuit voltage (V_{OC}) of PSCs. The frequency is varied from 5 Hz to 105 Hz. Capacitance-voltage (C-V) testing was also performed using the same setup. The transient photocurrent (TPC) measurement was done by the homemade setup in our laboratory.[5,15,31,32]

3. RESULTS AND DISCUSSION

PPA, as shown in **Fig. 1a**, is a conjugated molecule used to create a discrete 2D $(PPA)_x(MAPbI_3)_{1-x}$ thin layer on the top of 3D $MAPbI_3$ thin film for generating the $(PPA)_x(MAPbI_3)_{1-x}/MAPbI_3$ bilayer thin films. **Fig. 1b** presents the UV-visible absorption spectra of $MAPbI_3$ thin film and the $(PPA)_x(MAPbI_3)_{1-x}/MAPbI_3$ bilayer thin film. Due to the quantum confinement, a slightly blue-shifted absorption spectrum is observed from the $(PPA)_x(MAPbI_3)_{1-x}/MAPbI_3$ bilayer thin film compared to $MAPbI_3$ thin film. Moreover, a

blue-shifted PL is also observed from the $(PPA)_x(MAPbI_3)_{1-x}/MAPbI_3$ bilayer thin film (774 nm) compared to that (780 nm) from $MAPbI_3$ thin film (**Figs. 1c** & **1d**). In addition, an emission peak located at 722 nm observed from the $(PPA)_x(MAPbI_3)_{1-x}/MAPbI_3$ bilayer thin film indicates the existence of $(PPA)_x(MAPbI_3)_{1-x}$ perovskite due to multiple *n* values coexisted in the system. All these results indicate that $(PPA)_x(MAPbI_3)_{1-x}$ is formed as a 2D perovskite structure.[33-35] In addition, compared to 3D $MAPbI_3$, obviously increased PL intensity observed in the $(PPA)_x(MAPbI_3)_{1-x}/MAPbI_3$ bilayer thin film (**Fig. S1**) indicates that non-radiative recombination within the $(PPA)_x(MAPbI_3)_{1-x}/MAPbI_3$ bilayer thin film was significantly suppressed.

The XRD patterns of $MAPbI_3$ thin film and the $(PPA)_x(MAPbI_3)_{1-x}/MAPbI_3$ bilayer thin film are shown in **Fig. 2a**. The (110) and (220) peaks at 2θ of ~14° and ~28°, respectively, demonstrate that both $MAPbI_3$ thin film and the $(PPA)_x(MAPbI_3)_{1-x}/MAPbI_3$ bilayer thin film possess the tetragonal (*I4/mcm*) crystal structure.[36] However, a peak located at 2θ of ~ 6.6°, corresponding to the (002) plane, is observed from the $(PPA)_x(MAPbI_3)_{1-x}/MAPbI_3$ bilayer thin film, which further confirms that $(PPA)_x(MAPbI_3)_{1-x}$ is formed as a 2D perovskite structure.[33-35] **Fig. 2b** shows the patterns of the (110) peaks for $MAPbI_3$ thin film and the $(PPA)_x(MAPbI_3)_{1-x}/MAPbI_3$ bilayer thin film. It is found that the $(PPA)_x(MAPbI_3)_{1-x}/MAPbI_3$ bilayer thin film possesses smaller full width at half maximum (FWHM) (0.201°) compared to that (0.309°) observed from $MAPbI_3$ thin film, indicating that the $(PPA)_x(MAPbI_3)_{1-x}/MAPbI_3$ bilayer thin film exhibits enlarged crystallinity.[37] Such enlarged crystallinity is attributed to the progressive trap healing at the grain boundaries and the passivated surface of thin film.[38,39]

Fig. 2c, d presents the SEM images of $MAPbI_3$ thin film and the $(PPA)_x(MAPbI_3)_{1-x}/MAPbI_3$ bilayer thin film. It is found that patches of a new phase with bright grain spots are observed from the $(PPA)_x(MAPbI_3)_{1-x}/MAPbI_3$ bilayer thin film compared to $MAPbI_3$ thin film. Such bright grain spots are originated from the lower electrical conductivity of the $(PPA)_x(MAPbI_3)_{1-x}/MAPbI_3$ bilayer thin film compared to $MAPbI_3$ thin film. All these characteristics further confirm that $(PPA)_x(MAPbI_3)_{1-x}$ is indeed formed as a 2D perovskite structure.[40]

To verify that conjugated molecule, PPA, could facilitate charge transport, the charge carrier mobility of the $(PPA)_x(MAPbI_3)_{1-x}/MAPbI_3$ bilayer thin film is investigated through the characterization of both electron-only and hole-only diodes based on the space charge limited current (SCLC) method, according to the Mott-Gurney law.[41-44] The electron-only diode with a device structure of ITO/SnO_2/active layer/C_{60}/Al and the hole-only diode with a device structure of ITO/PEDOT:PSS/active layer/MoO_3/Ag, where the active layer is either the $(PPA)_x(MAPbI_3)_{1-x}/MAPbI_3$ bilayer thin film or $MAPbI_3$ thin film, are fabricated and characterized. As shown in **Fig. 2e, f**, the J-V characteristics can be divided into the Ohmic region ($J \propto V$) under the low bias and the SCLC region ($J \propto V^2$) under high bias. The J-V curve at the SCLC region could be well-fitted by the Mott-Gurney law: $J = \frac{9\varepsilon\varepsilon_0\mu V^2}{8L^3}$ (where μ is the charge carrier mobility, V is the external bias and L is the thickness of perovskite thin film, ε_0 is the vacuum permittivity and ε is the dielectric constant for perovskite thin film).[41-44] Based on the capacitance versus frequency (C-V) characteristics of perovskite thin films (**Fig. S2**), the ε values are calculated to be 26.6 and 25.4 for the $(PPA)_x(MAPbI_3)_{1-x}/MAPbI_3$ bilayer thin film and $MAPbI_3$ thin film, respectively. Therefore,

the charge carrier mobilities of $MAPbI_3$ thin film are calculated to be 6.52×10^{-4} $cm^2V^{-1}s^{-1}$ (electron mobility) and 1.43×10^{-3} $cm^2V^{-1}s^{-1}$ (hole mobility), respectively. These values are consistent with the reported values.[45,46] Furthermore, these charge carrier mobility values indicate that the charge transport is unbalanced ($\mu e/\mu h = 0.46$) within $MAPbI_3$ thin film. The charge carrier mobilities for the $(PPA)_x(MAPbI_3)_{1-x}/MAPbI_3$ bilayer thin film are calculated to be 7.52×10^{-3} $cm^2V^{-1}s^{-1}$ (electron mobility) and 8.24×10^{-3} $cm^2V^{-1}s^{-1}$ (hole mobility), respectively. Both hole mobility and electron mobility of the $(PPA)_x(MAPbI_3)_{1-x}/MAPbI_3$ bilayer thin film are higher than those from $MAPbI_3$ thin film. Such boosted charge carrier mobility is attributed to a conjugated chain of PPA as compared with insulating organic spacers.[22-28] Moreover, these charge carrier mobility values indicate that the charge transport is tended to be balanced ($\mu e/\mu h = 0.90$). As a result, enhanced J_{SC} is expected to be observed from PSCs by the $(PPA)_x(MAPbI_3)_{1-x}/MAPbI_3$ bilayer thin film.

The photovoltaic properties of the $(PPA)_x(MAPbI_3)_{1-x}/MAPbI_3$ bilayer thin film are investigated through the characterization of the PSCs with a device structure of ITO/PTAA/perovskite/C_{60}/BCP/Al, where ITO acts as the anode, PTAA acts as the hole extraction layer (HEL), C_{60} is used as the electron extraction layer (EEL) and the hole blocking layer (HBL), BCP is used as another HBL, Al acts as the cathode, respectively. **Fig. 3a** presents the statistics of PCEs of the PSCs by the $(PPA)_x(MAPbI_3)_{1-x}/MAPbI_3$ bilayer thin films with different PPA concentrations. The PCEs values of PSCs are increased and then decreased along with increased concentrations of PPA. At the concentration of PPA is at 0.5 %, the PSCs by the $(PPA)_x(MAPbI_3)_{1-x}/MAPbI_3$ bilayer thin film exhibit the best PCEs. The J-V characteristics of the PSCs by either $MAPbI_3$ thin film or the

$(PPA)_x(MAPbI_3)_{1-x}/MAPbI_3$ bilayer thin films (x=0.5%) are shown in **Fig. 3b.** The PSCs by $MAPbI_3$ thin film exhibit a short-circuit current density (J_{SC}) of 21.41 mA cm^{-2}, a V_{OC} of 1.04 V, and a fill factor (FF) of 78%, with a corresponding PCE of 17.37%. These device performance parameters are consistent with reported values.[47] The PSCs by the $(PPA)_x(MAPbI_3)_{1-x}/MAPbI_3$ bilayer thin film exhibit a J_{SC} of 25.92 mA cm^{-2}, a V_{OC} of 1.06 V, a FF of 80%, and with a corresponding PCE of 21.98%, which is approximatively 25 % enhancement compared to that by $MAPbI_3$ thin film. Such boosted PCE is ascribed to the conjugated PPA organic spacer with better charge transport property in comparison with insulating molecules such as butyl amine and benzene-based amine.[19-28] **Fig. 3c** shows the EQE spectra of PSCs. The PSCs by the $(PPA)_x(MAPbI_3)_{1-x}/MAPbI_3$ bilayer thin film exhibit enhanced EQE values compared to that by $MAPbI_3$ thin film. The integrated current densities are 20.89 mA cm^{-2} and 25.24 mA cm^{-2} for the PSCs by $MAPbI_3$ thin film and the PSCs by the $(PPA)_x(MAPbI_3)_{1-x}/MAPbI_3$ bilayer thin film, respectively. These integrated current densities are in good agreement with J_{SC} values obtained from the J-V characteristics (**Fig. 3b**).

The stability of un-encapsulated PSCs measured in the ambient atmosphere (25 °C and 30 ± 10 humidity) is shown in **Fig. 3d.** The PSCs by the $(PPA)_x(MAPbI_3)_{1-x}/MAPbI_3$ bilayer thin film retains 50% of their initial PCEs after 1200 hours (hrs), whereas the PSCs by $MAPbI_3$ thin film shows a significant degradation after 100 hrs and degrades more than 50% of their original PCEs after 500 hrs. The conjugated long-chain cations PPA could anchor on the surface of the perovskite grain boundary, which could passivate trap states, resulting in robust $(PPA)_x(MAPbI_3)_{1-x}/MAPbI_3$ bilayer thin film to sustain moisture and oxygen. In addition, the

enhanced stability of PSCs is attributed to the pinhole-free thin film of the $(PPA)_x(MAPbI_3)_{1-x}/MAPbI_3$ bilayer thin film.

To understand the underlying physics of enhanced J_{SC}, the TPC measurement is carried out to probe photogenerated charge transport rather than just measure the photocurrent.[32] **Fig. 4a** presents the TPC curves of PSCs. As an external bias of -1.0 V is applied across PSCs to minimize charge carrier recombination, the charge carrier extraction time is estimated by extrapolating the photocurrent density to zero from the linear regime.[32] Based on the normalized TPC curves, the charge carrier extraction times are estimated to be ~ 90 ns and ~70 ns for the PSCs by $MAPbI_3$ thin film and the PSCs by the $(PPA)_x(MAPbI_3)_{1-x}/MAPbI_3$ bilayer thin film, respectively. A short charge carrier extraction time indicates that an efficient charge extraction process takes place in solar cells.[32] Thus, the PSCs by the $(PPA)_x(MAPbI_3)_{1-x}/MAPbI_3$ bilayer thin film exhibit higher J_{SC}.

The light intensity-dependent J_{SC} and V_{OC} are investigated for visualization of the charge carrier recombination loss mechanisms in PSCs. As indicated in **Fig. 4b**, both PSCs follow the relationship of $V_{OC} \propto S \ln(I)$[48] (where $S = nk_BT/q$, k_B is the Boltzmann constant, T is the absolute temperature and q is the elementary charge, and I is the light intensity, respectively). An $S = 1.56\ k_BT/q$ observed from the PSCs by $MAPbI_3$ thin film indicates that both bimolecular charge carrier recombination and trap-assistant charge carrier recombination occurred in PSCs; whereas an $S = 1.11\ k_BT/q$ observed from the PSCs by the $(PPA)_x(MAPbI_3)_{1-x}/MAPbI_3$ bilayer thin film indicates that the trap-assistant charge carrier recombination within PSCs is suppressed. Furthermore, based on $J_{SC} \propto I^{\alpha}$ (where I is the light intensity and α is the coefficient),[48] both PSCs exhibit a power-law dependence of J_{SC}

on the light intensity. As $\alpha = 1$, all charge carriers are swept out before recombination. α of 0.83 and 0.94 are observed from the PSCs by $MAPbI_3$ thin film and the PSCs by the $(PPA)_x(MAPbI_3)_{1-x}/MAPbI_3$ bilayer thin film, respectively. A large α suggests that the bimolecular recombination is suppressed. Thus, the PSCs by the $(PPA)_x(MAPbI_3)_{1-x}/MAPbI_3$ bilayer thin film exhibit boosted J_{SC} compared to that by $MAPbI_3$ thin film.

The IS is applied to investigate the charge transport and recombination processes within PSCs.[49] As indicated in **Fig. 4c**, the charge carrier recombination resistances (R_{rec}) for the PSCs by $MAPbI_3$ thin film and the PSCs by the $(PPA)_x(MAPbI_3)_{1-x}/MAPbI_3$ bilayer thin film measured in dark are estimated to be ~ 440 Ω, and ~ 720 Ω, respectively. A high R_{rec} indicates a weak charge carrier recombination takes place in PSCs. Thus, the PSCs by the $(PPA)_x(MAPbI_3)_{1-x}/MAPbI_3$ bilayer thin film exhibit higher J_{SC}. The charge transfer resistance (R_{CT}) values are further calculated from the *IS* spectra at low frequency measured under white light illumination (**Fig. 4c)**. The R_{CT} for the PSCs by the $(PPA)_x(MAPbI_3)_{1-x}/MAPbI_3$ bilayer thin film is calculated to be ~ 80 Ω, whereas an R_{CT} of ~ 130 Ω is calculated for the PSCs by $MAPbI_3$ thin film. A small R_{CT} indicates that charge transport properties of PSCs are boosted, thereby resulting in an enhanced J_{SC}.[50]

The Mott-Schottky analysis, based on the C-V measurement, is further carried out to investigate the built-in potentials (V_{bi}) of PSCs [50]. As shown in **Fig. 4d**, under the forward bias, the V_{bi} of PSCs is extracted from $C^{-2} = \frac{2(V_{bi} - V)}{q\varepsilon\varepsilon_0 A^2 n_{trap}}$,[48] (where ε is the dielectric constant, ε_0 is the vacuum permittivity and A is the active area) by extrapolating the linear fitting line to the intercept on the *x*-axis. It is found that V_{bi} of ~1.15 V is observed from the PSCs by the $(PPA)_x(MAPbI_3)_{1-x}/MAPbI_3$ bilayer thin film, whereas a V_{bi} of ~1.09 V is observed from

the PSCs by $MAPbI_3$ thin film. Therefore, as expected, the PSCs by the $(PPA)_x(MAPbI_3)_{1-x}/MAPbI_3$ bilayer thin film exhibit a larger V_{OC} compared to that by $MAPbI_3$ thin film.

4. CONCLUSIONS

In conclusion, an innovative conjugated aniline PPA used to create 2D $(PPA)_x(MAPbI_3)_{1-x}$ thin layer and further form the $(PPA)_x(MAPbI_3)_{1-x}/MAPbI_3$ bilayer thin film for approaching efficient and stable perovskite solar cells were reported in this study. Systematically studies indicated that the $(PPA)_x(MAPbI_3)_{1-x}/MAPbI_3$ bilayer thin film possessed higher crystallinity and passivated trap states, resulting in improved charge carrier transport and suppressed charge carrier recombination with respective to $MAPbI_3$ thin film. As a result, the PSCs by the $(PPA)_x(MAPbI_3)_{1-x}/MAPbI_3$ bilayer thin film exhibited a PCE of 21.98 % and significantly boosted stability in the ambient atmosphere. Our results suggested that the utilization of conjugated molecules as organic spacer cations to create 2D perovskites and further form 2D/3D perovskite bilayer thin film is an effective way to approach high-performance PSCs.

CONFLICT OF INTEREST

There are no conflicts to declare.

ACKNOWLEDGMENTS

The authors acknowledge the National Science Foundation (ECCS/EPMD1903303) and Air Force Office of Scientific Research (AFOSR) (through the Organic Materials Chemistry Program, Grant Number: FA9550-15-1-0292, Program Manager, Dr. Kenneth Caster) for financial supports.

REFERENCES

1 A. Kojima, K. Teshima, Y. Shirai and T. Miyasaka, *J. Am. Chem. Soc.*, 2009, **131**, 6050-6051. DOI: 10.1021/ja809598r.

2 M. M. Lee, J. Teuscher, T. Miyasaka, T. N. Murakami and H. J. Snaith, *Science*, 2012, **338**, 643-647. DOI: 10.1126/science.1228604.

3 J. H. Heo, S. H. Im, J. H. Noh, T. N. Mandal, C. -S. Lim, J. A. Chang, Y. H. Lee, H.-J. Kim, A. Sarkar and M. K. Nazeeruddin, *Nat. Photonics*, 2013, **7**, 486-491. DOI: 10.1038/nphoton.2013.80.

4 H. J. Snaith, *J. Phys. Chem. Lett.*, 2013, **4**, 3623-3630. DOI: 10.1021/jz4020162.

5 K. Wang, L. Zheng, T. Zhu, L. Liu, M. L. Becker and X. Gong, *Nano Energy*, 2020, **67**, 104229. DOI: 10.1016/j.nanoen.2019.104229.

6 K. Wang, L. Zheng, T. Zhu, X. Yao, C. Yi, X. Zhang, Y. Cao, L. Liu, W. Hu and X. Gong, *Nano Energy*, 2019, **61**, 352-360. DOI: 10.1016/j.nanoen.2019.04.073.

7 W. Xu, L. Zheng, T. Zhu, L. Liu and X. Gong, *ACS Appl. Mater. Interfaces*, 2019, **11**, 34020-34029. DOI: 10.1021/acsami.9b12346.

8 L. Dou, Y. M. Yang, J. You, Z. Hong, W.-H. Chang, G. Li and Y. Yang, *Nat. Commun.*, 2014, **5**, 1-6. DOI: 10.1038/ncomms6404.

9 C. Liu, K. Wang, P. Du, E. Wang, X. Gong and A. J. Heeger, *Nanoscale*, 2015, **7**, 16460-16469. DOI: 10.1039/C5NR04575D.

10 T. Zhu, Y. Yang, L. Zheng, L. Liu, M. L. Becker and X. Gong, *Adv. Funct. Mater.*, 2020, **30**, 1909487. DOI: 10.1002/adfm.201909487.

11 W. Xu, Y. Guo, X. Zhang, L. Zheng, T. Zhu, D. Zhao, W. Hu and X. Gong, *Adv. Funct. Mater.*, 2018, **28**, 1705541. DOI: 10.1002/adfm.201705541.

12 N. NREL, US Department of Energy, 2019. https://www.nrel.gov/pv/cell-efficiency.html

13 G. Niu, X. Guo and L. Wang, *J. Mater. Chem. A*, 2015, **3**, 8970-8980. DOI: 10.1039/C4TA04994B.

14 C. J. Bartel, C. Sutton, B. R. Goldsmith, R. Ouyang, C. B. Musgrave, L. M. Ghiringhelli and M. Scheffler, *Sci. adv.*, 2019, **5**, eaav0693. DOI: 10.1126/sciadv.aav0693.

15 T. Zhu, Y. Yang, K. Gu, C. Liu, J. Zheng and X. Gong, *ACS Appl. Mater. Interfaces*, 2020, **12**, 51744-51755. DOI: 10.1021/acsami.0c16514.

16 Y. Bai, S. Xiao, C. Hu, T. Zhang, X. Meng, H. Lin, Y. Yang and S. Yang, *Adv. Energy Mater.*, 2017, **7**, 1701038. DOI: 10.1002/aenm.201701038.

17 Q. He, M. Worku, L. Xu, C. Zhou, H. Lin, A. J. Robb, K. Hanson, Y. Xin and B. Ma, *ACS Appl. Mater. Interfaces*, 2019, **12**, 1159-1168. DOI: 10.1021/acsami.9b17851.

18 J. Y. Ye, J. Tong, J. Hu, C. Xiao, H. Lu, S. P. Dunfield, D. H. Kim, X. Chen, B. W. Larson, J. Hao, K. Wang, Q. Zhao, Z. Chen, H. Hu, W. You, J. J. Berry, F. Zhang and K. Zhu, *Sol. RRL*, 2020, **4**, 2000082. DOI: 10.1002/solr.202000082.

19 Q. Jiang, Y. Zhao, X. Zhang, X. Yang, Y. Chen, Z. Chu, Q. Ye, X. Li, Z. Yin and J. You, *Nat. Photonics*, 2019, **13**, 460-466. DOI: 10.1038/s41566-019-0398-2.

20 F. Wang, W. Geng, Y. Zhou, H. H. Fang, C. J. Tong, M. A. Loi, L. M. Liu and N. Zhao, *Adv. Mater.*, 2016, **28**, 9986-9992. DOI: 10.1002/adma.201603062.

21 T. Zhou, H. Lai, T. Liu, D. Lu, X. Wan, X. Zhang, Y. Liu and Y. Chen, *Adv. Mater.*, 2019, **31**, 1901242. DOI: 10.1002/adma.201901242.

22 L. Mao, C. C. Stoumpos and M .G. Kanatzidis, *J. Am. Chem. Soc.*, 2018, **141**, 1171-1190. DOI: 10.1021/jacs.8b10851.

23 L. Mao, W. Ke, L. Pedesseau, Y. Wu, C. Katan, J. Even, M. R. Wasielewski, C. C. Stoumpos and M. G. Kanatzidis, *J. Am. Chem. Soc.*, 2018, **140**, 3775-3783. DOI: 10.1021/jacs.8b00542.

24 N. Zhou, B. Huang, M. Sun, Y. Zhang, L. Li, Y. Lun, X. Wang, J. Hong, Q. Chen and H. Zhou, *Adv. Energy Mater.*, 2020, **10**, 1901566. DOI: 10.1002/aenm.201901566.

25 Y. Zhang, J. Chen, X. Lian, M. Qin, J. Li, T. R. Andersen, X. Lu, G. Wu, H. Li and H. Chen, *Small Methods*, 2019, **3**, 1900375. DOI: 10.1002/smtd.201900375.

26 D. H. Cao, C. C. Stoumpos, O. K. Farha, J. T. Hupp and M. G. Kanatzidis, *J. Am. Chem. Soc.*, 2015, **137**, 7843-7850. DOI: 10.1021/jacs.5b03796.

27 J. Qiu, Y. Xia, Y. Zheng, W. Hui, H. Gu, W. Yuan, H. Yu, L. Chao, T. Niu, Y. Yang, X. Gao, Y. Chen and W. Huang, *ACS Energy Lett.*, 2019, **4**, 1513-1520. DOI: 10.1021/acsenergylett.9b00954.

28 F. Zhang, D. H. Kim, H. Lu, J .-S. Park, B. W. Larson, J. Hu, L. Gao, C. Xiao, O. G. Reid, X. Chen, Q. Zhao, P. F. Ndione, J. J. Berry, W. You, A. Walsh, M C. Beard and K. Zhu, *J. Am. Chem. Soc.*, 2019, **141**, 5972-5979. DOI: 10.1021/jacs.9b00972.

29 K. Wang, J. Liu, J. Yin, E. Aydin, G. T. Harrison, W. Liu, S. Chen, O. F. Mohammed and S. De Wolf, *Adv. Funct. Mater.*, 2020, **30**, 2002861. DOI: 10.1002/adfm.202002861.

30 M. Zhang, S. Dai, S. Chandrabose, K. Chen, K. Liu, M. Qin, X. Lu, J.M. Hodgkiss, H. Zhou and X. Zhan, *J. Am. Chem. Soc.*, 2018, **140**, 14938-14944. DOI: 10.1021/jacs.8b09300.

31 T. Zhu, L. Zheng, Z. Xiao, X. Meng, L. Liu, L. Ding and X. Gong, *Sol. RRL*, 2019, **3**, 1900322. DOI: 10.1002/solr.201900322.

32 J. Seifter, Y. Sun and A.J. Heeger, *Adv. Mater.*, 2014, **26**, 2486-2493. DOI: 10.1002/adma.201305160.

33 J. Sun, N. Chandrasekaran, C. Liu, A. D. Scully, W. Yin, C. K. Ng and J. J. Jasieniak, *ACS Appl. Energy Mater.*, 2020, **3**, 8205-8215. DOI: 10.1021/acsaem.0c00553.

34 G. Liu, X. -X. Xu, S. Xu, L. Zhang, H. Xu, L. Zhu, X. Zhang, H. Zheng and X. Pan, *J. Mater. Chem. A*, 2020, **8**, 5900-5906. DOI: 10.1039/C9TA14139A

35 Z. Wang, Q. Lin, F. P. Chmiel, N. Sakai, L. M. Herz and H. J. Snaith, *Nat. Energy*, 2017, **2**, 1-10. DOI: 10.1038/nenergy.2017.135.

36 T. Oku, *Solar Cells-New Approaches and Reviews*, 2015. DOI: 10.5772/59284.

37 V. Pecharsky and P. Zavalij, *Fundamentals of powder diffraction and structural characterization of materials*, Springer Science & Business Media, 2008.

38 D. -Y. Son, J. -W. Lee, Y. J. Choi, I. -H. Jang, S. Lee, P. J. Yoo, H. Shin, N. Ahn, M. Choi, D. Kim and N. -G. Park, *Nat. Energy*, 2016, **1**, 1-8. DOI: 10.1038/nenergy.2016.81.

39 N. Phung, A. Al-Ashouri, S. Meloni, A. Mattoni, S. Albrecht, E. L. Unger, A. Merdasa and A. Abate, *Adv. Energy Mater.*, 2020, **10**, 1903735. DOI: 10.1002/aenm.201903735.

40 D. Kim, H. J. Jung, I. J. Park, B. W. Larson, S. P. Dunfield, C. Xiao, J. Kim, J. Tong, P. Boonmongkolras, S. G. Ji, F. Zhang, S. R. Pae, M. Kim, S. B. Kang, V. Dravid, J. J. Berry, J. Y. Kim, K. Zhu, D. H. Kim and B. Shin, *Science*, 2020, **368**, 155-160. DOI: 10.1126/science.aba3433.

41 R. H. Bube, *J. Appl. Phys.*, 1962, **33**, 1733-1737. DOI: 10.1063/1.1728818.

42 E. A. Duijnstee, J. M. Ball, V. M. Le Corre, L. J. A. Koster, H. J. Snaith and J. Lim, *ACS Energy Lett.*, 2020, **5**, 376-384. DOI: 10.1021/acsenergylett.9b02720.

43 X. Zhang, X. Ren, B. Liu, R. Munir, X. Zhu, D. Yang, J. Li, Y. Liu, D.-M. Smilgies, R. Li, Z. Yang, T. Niu, X. Wang, A. Amassian, K. Zhao and S. F. Liu, *Energy Environ. Sci.*, 2017, **10**, 2095-2102. DOI: 10.1039/C7EE01145H.

44 P. Murgatroyd, *J. Phys. D Appl. Phys.*, 1970, **3**, 151. DOI: 10.1088/0022-3727/3/2/308.

45 G. Xing, N. Mathews, S. S. Lim, N. Yantara, X. Liu, D. Sabba, M. Grätzel, S. Mhaisalkar and T. C. Sum, *Nat. Mater.*, 2014, 13, 476-480. DOI: 10.1038/nmat3911.

46 L. M. Herz, *ACS Energy Lett.*, 2017, **2**, 1539-1548. DOI: 10.1021/acsenergylett.7b00276.

47 A. Mahapatra, D. Prochowicz, M. M. Tavakoli, S. Trivedi, P. Kumar and P. Yadav, *J. Mater. Chem. A*, 2020, **8**, 27-54. DOI: 10.1039/C9TA07657C.

48 F. Fabregat-Santiago, G. Garcia-Belmonte, I. Mora-Sero and J. Bisquert, *Phys. Chem. Chem. Phys.*, 2011, **13**, 9083-9118. DOI: 10.1039/C0CP02249G.

49 T. Zhu, Y. Yang, Y. Liu, R. Lopez-Hallman, Z. Ma, L. Liu and X. Gong, *Nano Energy*, 2020, **78**, 105397. DOI: 10.1016/j.nanoen.2020.105397.

50 S. R. Cowan, A. Roy and A.J. Heeger, *Phys. Rev. B*, 2010 **82**, 245207. DOI: 10.1103/PhysRevB.82.245207.

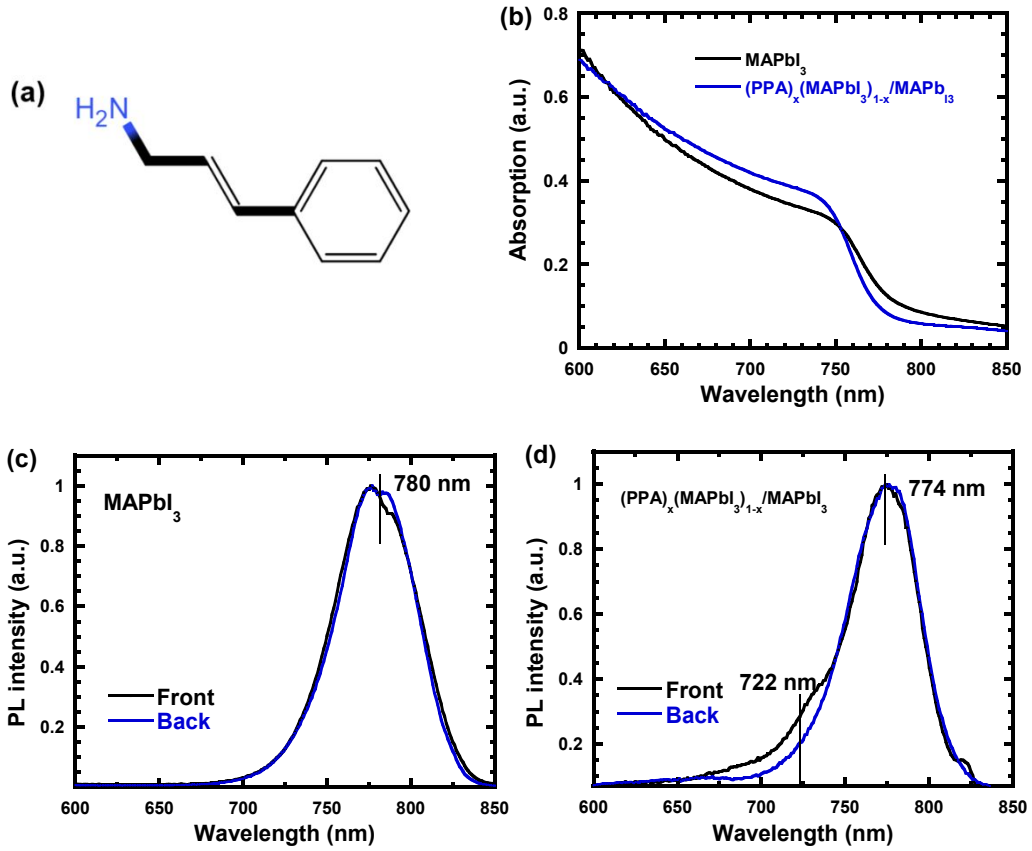

Fig. 1 (a) The molecular structure of PPA. (b) The absorption spectra of $MAPbI_3$ and $(PPA)_x(MAPbI_3)_{1-x}/MAPbI_3$ thin films. The PL spectra of (c) $MAPbI_3$ and (d) $(PPA)_x(MAPbI_3)_{1-x}/MAPbI_3$ thin films from front side and back side.

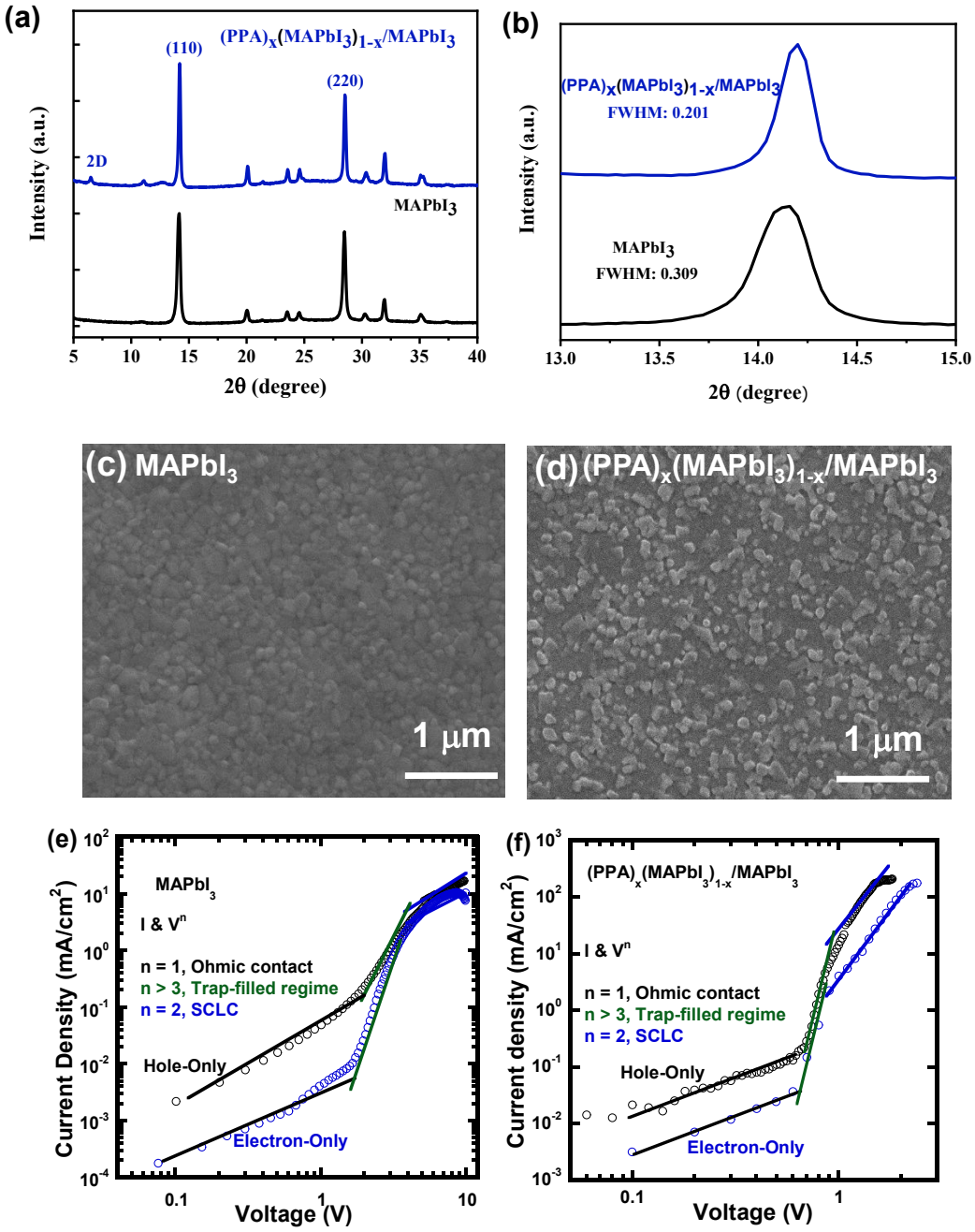

Fig. 2 (a) XRD patterns of $MAPbI_3$ and $(PPA)_x(MAPbI_3)_{1-x}/MAPbI_3$ thin films, (b) magnified the (110) peak of XRD patterns. Top-view SEM images of (c) $MAPbI_3$ and (d) $(PPA)_x(MAPbI_3)_{1-x}/MAPbI_3$ thin films, and the current density versus of voltage characteristics of diodes fabricated by (e) $MAPbI_3$ and (f) $(PPA)_x(MAPbI_3)_{1-x}/MAPbI_3$ thin films, respectively.

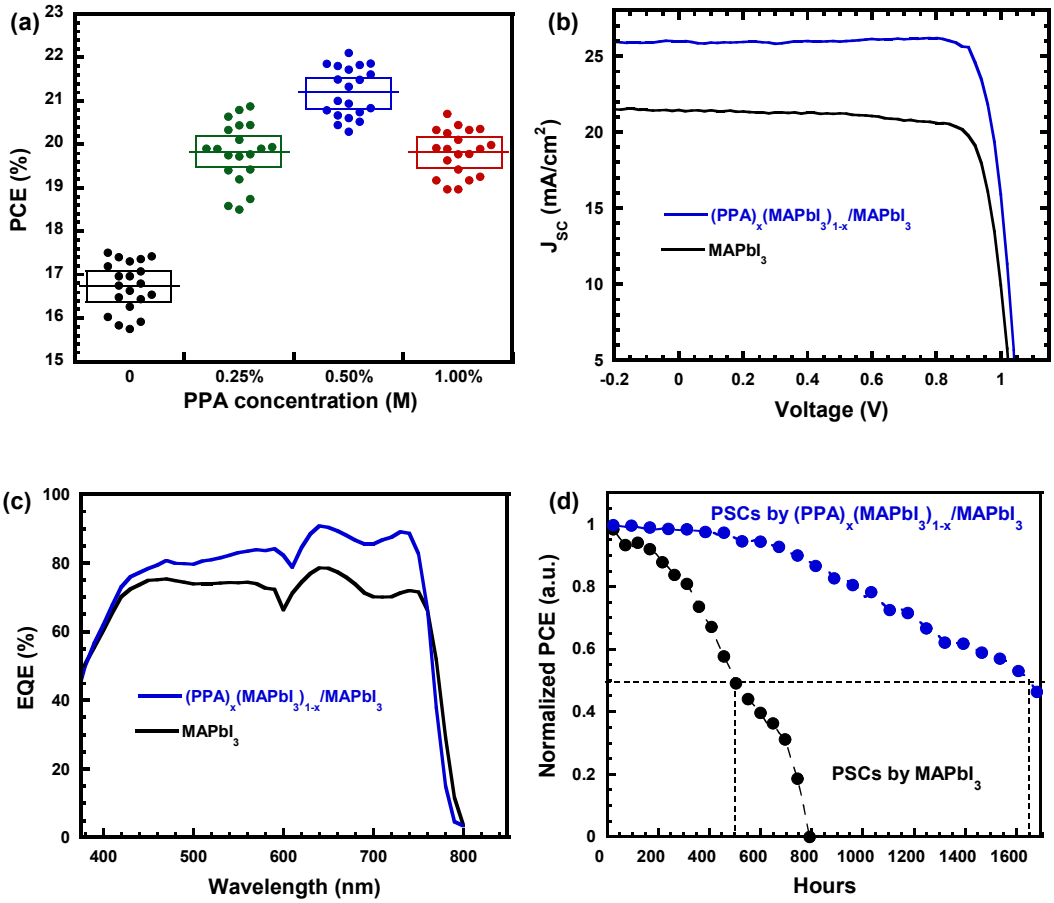

Fig. 3 (a) The statistics of PCEs of PSCs by $(PPA)_x(MAPbI_3)_{1-x}$/ $MAPbI_3$ thin films with different PPA concentrations. (b) The J-V characteristics and (c) EQE spectra of PSCs by either $MAPbI_3$ or $(PPA)_x(MAPbI_3)_{1-x}/MAPbI_3$ thin films. (d) The stabilities of PSCs by either $MAPbI_3$ thin film or $(PPA)_x(MAPbI_3)_{1-x}/MAPbI_3$ thin film.

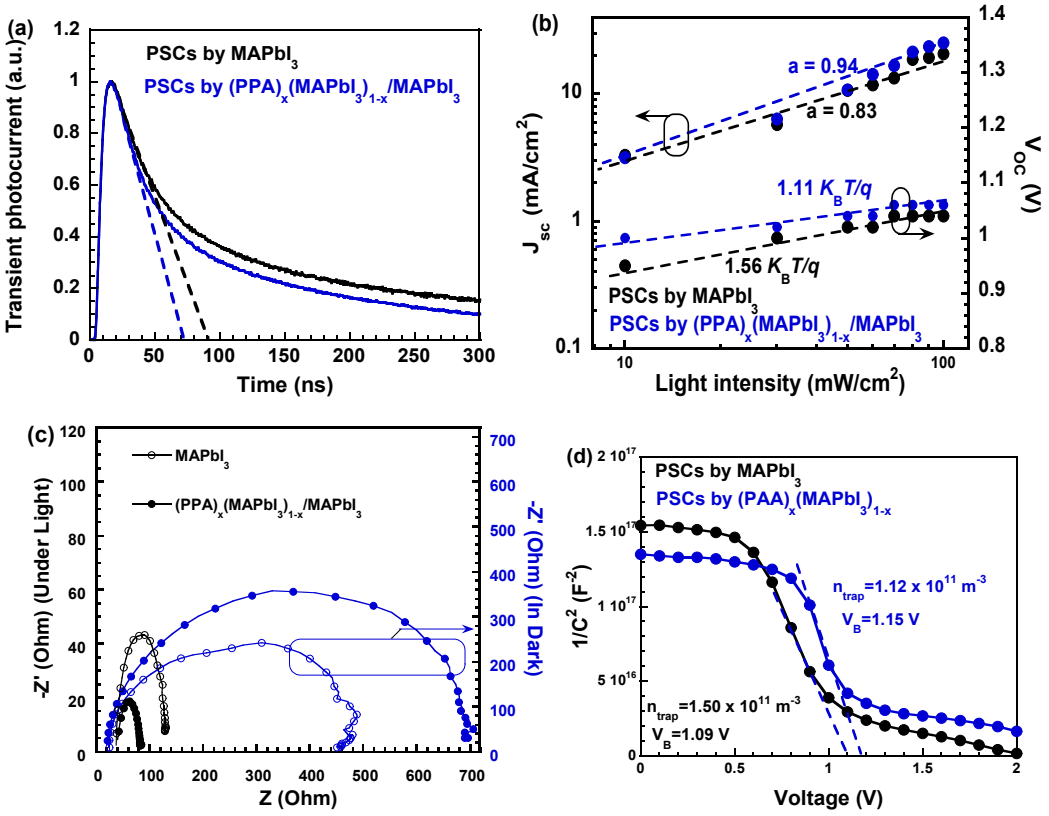

Fig. 4 (a) The normalized transient photocurrent (TPC) curve of PSCs by either $MAPbI_3$ thin film or $(PPA)_x(MAPbI_3)_{1-x}/MAPbI_3$ thin film. (b) V_{OC} and J_{SC} versus light intensity of PSCs by either $MAPbI_3$ thin film or $(PPA)_x(MAPbI_3)_{1-x}$/ $MAPbI_3$ thin film. (c) Nyquist plots of PSCs by either $MAPbI_3$ thin film or $(PPA)_x(MAPbI_3)_{1-x}/MAPbI_3$ thin film, measured in the dark, and (d) the Mott-Schottky analysis of PSCs.